β–$RhPb_2$: A topological superconductor candidate

Jian-Feng Zhang,[1] Peng-Jie Guo,[1] Miao Gao,[2] Kai Liu,[1,*] and Zhong-Yi Lu[1,†]

[1]*Department of Physics and Beijing Key Laboratory of Opto-electronic Functional Materials & Micro-nano Devices, Renmin University of China, Beijing 100872, China*

[2]*Department of Microelectronics Science and Engineering, Faculty of Science, Ningbo University, Zhejiang 315211, China*

(Received 30 July 2018; published 4 January 2019)

A topological superconductor candidate β-$RhPb_2$ is predicted by using first-principles electronic structure calculations. Our calculations show that there is a band inversion around the Fermi level at the Z point of Brillouin zone. The calculated nonzero topological invariant Z_2 indicates that β-$RhPb_2$ is a topological insulator defined on a curved Fermi level. Slab calculations further demonstrate that the gapless nontrivial topological surface states (TSS) are not overlapped by the bulk states and they cross the Fermi level. Phonon calculations confirm the dynamical stability of β-$RhPb_2$, while electron-phonon coupling (EPC) calculations predict that the superconducting transition temperature (T_c) of β-$RhPb_2$ can reach 9.7 K. The coexistence of nontrivial topological band structure with the TSS crossing the Fermi level as well as the superconducting T_c above the liquid-helium temperature suggest that the layered compound β-$RhPb_2$ is a topological superconductor, which deserves further experimental verification.

DOI: 10.1103/PhysRevB.99.045110

I. INTRODUCTION

Topological superconductor, characterized by a superconducting gap in bulk and Majorana zero modes at boundaries, has attracted great attention recently. The Majorana zero mode is a kind of special quasiparticle that is its own antiparticle and obeys non-Abelian statistics, and it possesses potential applications in topological quantum computation [1–3]. Theoretically, as an intrinsic topological superconductor, the spinless $p+ip$ type superconductor can hold Majorana zero modes at the vortices. Nevertheless, the reported p-wave superconductor candidates are very scarce [4]. On the other hand, it has been proposed that topological superconductivity can be realized in an equivalent $p+ip$ type superconductor [5,6], such as the interface of a heterostructure consisting of a topological insulator (TI) and an s-wave conventional superconductor [7,8], where the proximity effect can induce superconductivity in the spin-helical topological surface states (TSS) [5,6]. Such an approach, however, puts forward great challenges in preparing high-quality heterostructures and in observing the interface-related phenomena.

To avoid these difficulties in heterostructures, an alternative approach to realize topological superconductivity is to search for equivalent $p+ip$ type superconductivity in a single compound besides the spinless p-wave superconductors. In such a single compound, the bulk is an s-wave superconductor and meanwhile the surface hosts topological surface states that cross the Fermi level. The spin-helical topological surface states with spin-moment locking can be regarded being spinless, so the corresponding surface superconductivity induced by the superconducting proximity effect is effectively of p wave in order to abide by the pair-wave function antisymmetry [9]. In general, there are two strategies to search for single-compound topological superconductors. The first one is to induce superconductivity in a topological insulator by charge doping as in Cu/Sr/Nb-doped Bi_2Se_3 [10–12] and In-doped SnTe [13]. The second one is to examine the topological property of existing superconductors, such as in β-$PdBi_2$ [14], $PdTe_2$ [15], $PbTaSe_2$ [16,17], $Fe(Te_{0.55}Se_{0.45})$ [18–21], and A15 superconductors [22]. Among them, β-$PdBi_2$ owns two groups of topological surface states, one of which shows a Dirac point located 2.4 eV below the Fermi level and within the bulk band gap [14]. This inspires us to explore other single-compound topological superconductor candidates isostructural to β-$PdBi_2$ with the Dirac point near the Fermi level.

In this work, starting from the lattice structure of β-$PdBi_2$ [14] and using first-principles electronic structure calculations, we predict a topological superconductor candidate β-$RhPb_2$, which possesses a nontrivial topological band structure and becomes superconducting below 9.7 K. The topological surface states on the $RhPb_2(001)$ surface cross the Fermi level and will give rise to a superconducting gap when the bulk becomes superconducting. Our theoretical predictions await experimental realization.

II. METHOD

We investigated the electronic structure, phonon spectra, and electron-phonon coupling of β-$RhPb_2$ based on density functional theory (DFT) [23,24] and density functional perturbation theory (DFPT) [25] calculations as implemented in the QUANTUM ESPRESSO (QE) package [26]. The interactions between electrons and nuclei were described by norm-conserving pseudopotentials [27]. For the exchange-correlation functional, the generalized gradient approximation

*kliu@ruc.edu.cn
†zlu@ruc.edu.cn

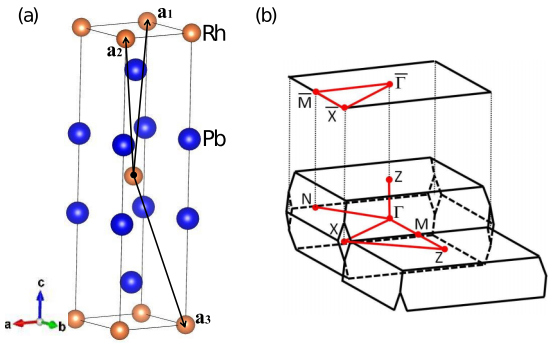

FIG. 1. (a) Crystal structure of bulk β-$RhPb_2$. The blue and orange balls represent the Pb and Rh atoms, respectively. The lattice vectors $\mathbf{a}_1$, $\mathbf{a}_2$, and $\mathbf{a}_3$ of a primitive cell are also indicated. (b) The Brillouin zone (BZ) of the primitive cell and the projected two-dimensional (2D) BZ of the (001) surface of β-$RhPb_2$. The high-symmetry paths in the BZ are indicated by the red lines.

(GGA) of Perdew-Burke-Ernzerhof (PBE) [28] type was adopted. The kinetic energy cutoff of the plane-wave basis was set to be 80 Ry. The van der Waals (vdW) interactions between the β-$RhPb_2$ layers were included by using the DFT-D2 method [29,30]. For the bulk calculations, we adopted a primitive cell with the corresponding lattice vectors $\mathbf{a}_1$, $\mathbf{a}_2$, and $\mathbf{a}_3$ shown in Fig. 1(a). A $12 \times 12 \times 12$ $\mathbf{k}$-point mesh was used for the Brillouin zone (BZ) [Fig. 1(b)] sampling of the primitive cell. For the Fermi surface broadening, the Gaussian smearing method with a width of 0.004 Ry was employed. In the structural optimization, both lattice constants and internal atomic positions were fully relaxed until the forces on atoms were smaller than 0.0002 Ry/bohr. To examine the possibility of magnetic moment introduced by Rh d orbitals, we studied three typical magnetic configurations for the square Rh lattice in β-$PdBi_2$, including the ferromagnetic state, the antiferromagnetic Néel state, and the single-stripe collinear antiferromagnetic state. After the self-consistent calculations, all these magnetic states converge to the nonmagnetic state without local magnetic moment on the Rh atom. The surface states in the two-dimensional (2D) Brillouin zone (BZ) of β-$RhPb_2$ were studied by using the WANNIERTOOLS package [31].

The superconducting transition temperature of β-$RhPb_2$ was studied based on the electron-phonon coupling (EPC) theory as implemented in the EPW package [32], which uses the maximally localized Wannier functions (MLWFs) [33] and interfaces with QE [26]. We took the $4 \times 4 \times 4$ for both $\mathbf{k}$-mesh and $\mathbf{q}$-mesh as the coarse grids and interpolated to the $72 \times 72 \times 72$ $\mathbf{k}$-mesh and $16 \times 16 \times 16$ $\mathbf{q}$-mesh dense grids, respectively. The EPC constant λ can be calculated either by the summation of the EPC constant $\lambda_{\mathbf{q}\nu}$ in the full BZ for all phonon modes or by the integral of the Eliashberg spectral function $\alpha^2F(\omega)$ [34], as

$$\lambda = \sum_{\mathbf{q}\nu} \lambda_{\mathbf{q}\nu} = 2 \int \frac{\alpha^2 F(\omega)}{\omega} d\omega. \tag{1}$$

The Eliashberg spectral function $\alpha^2F(\omega)$ is defined as

$$\alpha^2 F(\omega) = \frac{1}{2\pi N(\varepsilon_F)} \sum_{\mathbf{q}\nu} \delta(\omega - \omega_{\mathbf{q}\nu}) \frac{\gamma_{\mathbf{q}\nu}}{\hbar\omega_{\mathbf{q}\nu}}, \tag{2}$$

where $N(\varepsilon_F)$ is the density of states at the Fermi level ε_F, $\omega_{\mathbf{q}\nu}$ is the frequency of the νth phonon mode at the wave vector $\mathbf{q}$, and $\gamma_{\mathbf{q}\nu}$ is the phonon linewidth.

The superconducting transition temperature T_c can be predicted by substituting the EPC constant λ into the McMillan-Allen-Dynes formula [35,36],

$$T_c = f_1 f_2 \frac{\omega_{\log}}{1.2} \exp\left[\frac{-1.04(1+\lambda)}{\lambda(1-0.62\mu^*)-\mu^*}\right], \tag{3}$$

where μ^* is the effective screened Coulomb repulsion constant, $\omega_{\log}$ is the logarithmic average frequency,

$$\omega_{\log} = \exp\left[\frac{2}{\lambda}\int \frac{d\omega}{\omega}\alpha^2 F(\omega)\ln(\omega)\right], \tag{4}$$

and f_1 and f_2 are the correction factors when $\lambda > 1.3$, for which the detailed calculations were presented in Ref. [36]. In our calculation, μ^* was set to 0.1, in the range of the widely used empirical values of 0.08 to 0.15 [37,38].

III. RESULTS

Figure 1(a) shows a conventional cell of bulk β-$RhPb_2$. The β-$RhPb_2$ compound shares the same crystal structure as β-$PdBi_2$ with the space group $I4/mmm$ instead of the $CuAl_2$-type structure with the space group $I4/mcm$ [39]. Each Rh square lattice (labeled by orange atoms) is sandwiched by two Pb square lattices (labeled by blue atoms). The Rh atom locates at the center of eight Pb atoms, forming a $RhPb_2$ layer. Different $RhPb_2$ layers stack along the c direction with the AB sequence and constitute a body-centered-tetragonal (bct) structure. The optimized lattice constants are $a = b = 3.25$ Å and $c = 12.83$ Å, and the vertical distance between Pb atoms in the same $RhPb_2$ layer is 3.38 Å. The $\mathbf{a}_1$, $\mathbf{a}_2$, and $\mathbf{a}_3$ respectively indicate the lattice vectors of a primitive cell with the corresponding Brillouin zone (BZ) displayed in Fig. 1(b).

Figure 2 shows the calculated band structure of bulk β-$RhPb_2$ along the high-symmetry paths in the BZ of the primitive cell. The gray and red lines represent the results without and with the spin-orbit coupling (SOC), respectively. In the case without the SOC, there is a band crossing around the Z point near the Fermi level between the eighth and ninth bands, whose numbers are labeled at the right side of Fig. 2. These two crossing bands form a Dirac nodal ring (indicated by the blue circle), which is protected by mirror symmetry and/or both time-reversal and space-inversion symmetries. As both Rh and Pb are heavy elements [40], it is necessary to consider the SOC effect. Once the SOC is included, the crossing bands around the Z point gap out ($E_g \geqslant 0.5$ eV) and there appears a gap between the eighth and ninth bands in the whole Brillouin zone. Thus bulk β-$RhPb_2$ can be considered as an insulator defined on a curved Fermi level between the eighth and ninth bands. Given that there are both time-reversal and space-inversion symmetries in bulk β-$RhPb_2$, we can calculate its topological invariant Z_2 by the product of the parities of all the occupied bands at the eight time-reversal

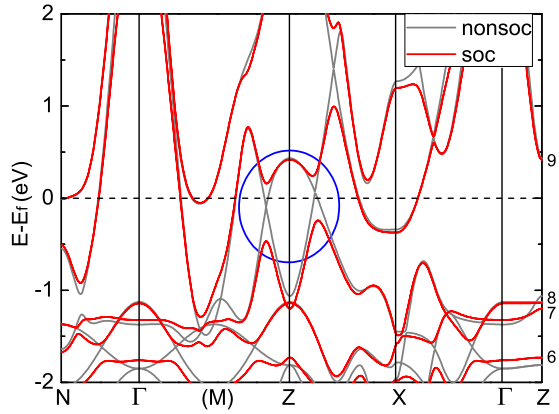

FIG. 2. Band structure of bulk β-$RhPb_2$ along the high-symmetry paths in the BZ defined in Fig. 1. The gray and red lines represent the results without and with the spin-orbit coupling (SOC), respectively. The blue circle emphasizes the band gap opening after including the SOC.

invariant momentum (TRIM) points [41], which respectively are one Γ point, two X points, four N points, and one Z point [Fig. 1(b)] for the BZ of the bct lattice. Since the numbers of the X and N points are even, only the parities of Γ and Z points decide the Z_2 topological invariant for β-$RhPb_2$. According to Table I, we know that the Z_2 invariant of bulk β-$RhPb_2$ equals 1, indicating its nontrivial topological properties. Further calculations adopting the modified Becke-Johnson (MBJ) potential [42,43] and the strongly constrained and appropriately normed (SCAN) functional [44,45] at the meta-GGA level give similar band structures and the same topological property, which validates our GGA results.

Besides the Z_2 topological invariant, the nontrivial topology can be also characterized through the surface states. Accordingly, we studied the surface states for the (001) surface of β-$RhPb_2$ (Fig. 3). Figures 2 and 3(a) show that the SOC-induced bulk band gap around the Z point is projected into the 2D BZ [Fig. 1(b)] mainly around the $\bar{\Gamma}$ point. In Fig. 3(a), the Dirac topological surface states protected by time-reversal symmetry locate in the bulk band gap and they pass through the Fermi level around the $\bar{\Gamma}$ point. This will contribute to the transport properties and will also increase their observability in angle-resolved photoemission spectroscopy (ARPES)

TABLE I. The parities of all the eight occupied bands of bulk β-$RhPb_2$ below the full gap at the eight time-reversal invariant momentum (TRIM) points in the BZ of the primitive cell.

Parity	Γ	$2X$	$4N$	Z
1	+	+	−	+
2	−	−	+	−
3	+	+	+	+
4	+	+	−	+
5	+	−	+	+
6	+	+	+	+
7	+	−	+	−
8	+	+	+	+
Total	−	−	+	+

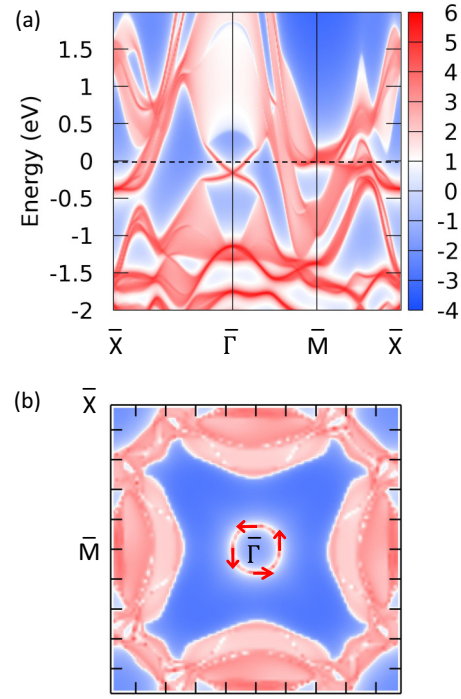

FIG. 3. (a) Band structure of the (001) surface of β-RhPb2 along the high-symmetry paths in the projected 2D BZ (Fig. 1). The Fermi energy E_F is set to zero. (b) Surface states in the 2D BZ at a fixed energy of E_F. Here arrows denote spin's directions. The topological surface states with the spin texture around the $\bar{\Gamma}$ point and within the bulk band gap can be clearly resolved.

experiments. The electronic states in the 2D BZ at a fixed energy of E_F are shown in Fig. 3(b), in which the topological surface states with the spin texture around the $\bar{\Gamma}$ point and within the bulk band gap can be clearly resolved. On the other hand, the electronic states around $\bar{X}$ and $\bar{M}$ points near the Fermi level contain both the projected bulk states in the 2D BZ and the topologically trivial surface states that are naturally extended from the bulk states. Once β-$RhPb_2$ becomes superconducting at low temperature, the topologically trivial states around $\bar{X}$ and $\bar{M}$ points will be gapped away from the Fermi level (s-wave superconductivity), while the spin-helical topological surface states around the $\bar{\Gamma}$ point will be induced into superconducting phase via the proximity effect and hold the equivalent $p + ip$ type superconductivity [5,6].

Considering that the β-$RhPb_2$ compound with the space group $I4/mmm$ (Fig. 1) has not been synthesized in experiment, we performed the phonon calculations to verify its dynamical stability. As shown in the phonon dispersion (left panel of Fig. 4), there is no imaginary frequency in the whole BZ except for only a tiny imaginary frequency (less than 1 meV) around the Γ point along the Γ–Z direction. The emergence of the tiny imaginary frequency around the Γ point can be interpreted as the difficulty of accurate interpolation in the long-range and low-frequency region. It is usually acceptable in layered materials and will not have influence on the following electron-phonon coupling (EPC) calculations.

We further performed EPC calculations with the SOC to study the superconducting properties of β-$RhPb_2$. The calculated total EPC constant λ of β-$RhPb_2$ is 1.76, indicating a

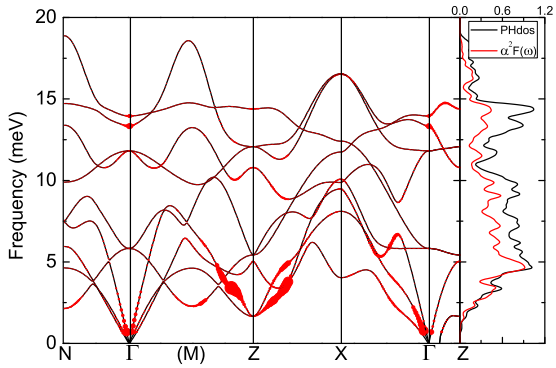

FIG. 4. Phonon dispersion for the primitive cell of bulk β-$RhPb_2$ calculated with the SOC. The sizes of red dots on black lines correspond to the strengths of electron-phonon coupling (EPC) $\lambda_{\mathbf{q}\nu}$. The right panel shows the phonon density of states (black line) and the Eliashberg spectral function $\alpha^2F(\omega)$ (red line).

strong EPC. In Fig. 4, the contributions to the EPC from the different phonon modes $\lambda_{\mathbf{q}\nu}$ are presented to be proportional to the sizes of red dots on the phonon dispersion lines (the left part). Obviously, the largest contribution comes from the acoustic branches around the Z point, which also results in several high peaks (around 3–5 meV) in the Eliashberg spectral function $\alpha^2F(\omega)$ (the right part of Fig. 4). Interestingly, the position of the **q** vector around the Z point, whose acoustic branch contributes most to λ (Fig. 4), is very similar to the position of the **k** vector for the nodal ring in the electronic band structure (Fig. 2). Through the Eliashberg spectral function $\alpha^2F(\omega)$ in Fig. 4 and Eq. (4), we obtain the logarithmic average of the phonon frequency, $\omega_{\log} = 7.86$ meV. Furthermore, based on the McMillan-Allen-Dynes formula [Eq. (3)], we predict the superconducting T_c of β-$RhPb_2$ to be 9.7 K, where the correction factors f_1 and f_2 are calculated to be 1.11 and 1.05, respectively. In the case without the SOC, the total EPC constant λ is 1.26 and the predicted T_c is 6.1 K. The reduced EPC constant λ in the absence of the SOC may originate from the giant influence of the SOC effect on the band structure around the Fermi level (Fig. 2).

To ascertain the reliability of our predicted superconducting T_c for β-$RhPb_2$, we have carried out a comparison study on the isostructural compound β-$PdBi_2$ with the same theoretical method. The calculated superconducting T_c of β-$PdBi_2$ is 4.5 K, which is close to the experimental value of 5.3 K [14]. On the other hand, we have also examined many other compounds isostructural to β-$PdBi_2$ but with three or four fewer valence electrons, including $RhGe_2$, $RhSn_2$, $IrGe_2$, $IrSn_2$, $IrPb_2$, $AgGa_2$, $AgIn_2$, $AgTl_2$, $AuGa_2$, $AuIn_2$, $AuTl_2$, $RuGe_2$, $RuSn_2$, $RuPb_2$, $OsGe_2$, $OsSn_2$, $OsPb_2$, $PtGa_2$, $PtIn_2$, $PtTl_2$, $PdGa_2$, $PdIn_2$, and $PdTl_2$. Unfortunately, these compounds are either dynamically unstable or hold predicted superconducting T_c below 3 K.

IV. DISCUSSION AND SUMMARY

A nontrivial topological band structure and a superconducting transition temperature of 9.7 K are predicted for the layered-structure compound β-$RhPb_2$ by using the first-principles electronic structure calculations. Due to the proximity effect, the bulk superconductivity will further induce superconductivity in the Dirac surface states. Such a superconductor is a topological superconductor, which is expected to hold Majorana zero modes at the vortices.

Compared with the reported potential topological superconductors, β-$RhPb_2$ has many advantages. First, as a topological superconductor, β-$RhPb_2$ avoids the difficulties in sample synthesis that occur in doped topological insulators and heterostructures, and eliminates the effects of disorder or distortion. Second, the superconducting transition temperature T_c of β-$RhPb_2$ (9.7 K) is above the liquid-helium temperature and higher than those of most other doped or intrinsic topological superconductor candidates: Cu/Sr/Nb-doped Bi_2Se_3 (below 4 K) [11,12,46], In-doped SnTe (below 4.6 K) [47,48], $PdTe_2$ (below 2 K) [15], $PbTaSe_2$ (3.8 K) [17], β-$PdBi_2$ (5.3 K) [14], and Ta_3Sb (0.7 K) [22]; however, the T_c of β-$RhPb_2$ is below that of $FeSe_{0.45}Te_{0.55}$ (14.5 K) [20]. Third, the giant SOC effect in β-$RhPb_2$ due to the heavy elements of component atoms induces a 0.5-eV band gap around the Z point of the 3D BZ (projected into the 2D BZ mainly around the $\bar{\Gamma}$ point) so that the inside topological surface states can be distinguished easily, which is conducive to observation in ARPES experiments.

In summary, a topological superconductor candidate β-$RhPb_2$ has been predicted by using first-principles electronic structure calculations. The nonzero topological invariant Z_2 of β-$RhPb_2$ indicates its nontrivial topological property. Based on EPC calculations, the superconducting transition temperature T_c of β-$RhPb_2$ is predicted to be 9.7 K. Since the nontrivial topological surface states cross the Fermi level without overlapping with the bulk states, the superconductivity in bulk β-$RhPb_2$ will further induce superconductivity in the TSS via the proximity effect. β-$RhPb_2$ may thus be an appropriate platform for exploring the exotic properties of topological superconductors and Majorana zero modes in experiment.

ACKNOWLEDGMENTS

We thank Z. X. Liu and X. Liu for helpful discussions. This work was supported by the National Key R&D Program of China (Grant No. 2017YFA0302903) and the National Natural Science Foundation of China (Grants No. 11774422 and No. 11774424). M.G. was supported by Zhejiang Provincial Natural Science Foundation of China (Grant No. LY17A040005). Computational resources were provided by the Physical Laboratory of High Performance Computing at Renmin University of China.

[1] C. Nayak, S. H. Simon, A. Stern, M. Freedman, and S. Das Sarma, Rev. Mod. Phys. **80**, 1083 (2008).
[2] X.-L. Qi and S.-C. Zhang, Rev. Mod. Phys. **83**, 1057 (2011).
[3] M. Sato and Y. Ando, Rep. Prog. Phys. **80**, 076501 (2017).
[4] A. P. Mackenzie and Y. Maeno, Rev. Mod. Phys. **75**, 657 (2003).
[5] L. Fu and C. L. Kane, Phys. Rev. Lett. **100**, 096407 (2008).

[6] X.-L. Qi, T. L. Hughes, S. Raghu, and S.-C. Zhang, Phys. Rev. Lett. **102**, 187001 (2009).

[7] M.-X. Wang, C. Liu, J.-P. Xu, F. Yang, L. Miao, M.-Y. Yao, C. L. Gao, C. Shen, X. Ma, X. Chen, Z.-A. Xu, Y. Liu, S.-C. Zhang, D. Qian, J.-F. Jia, and Q.-K. Xue, Science **336**, 52 (2012).

[8] J.-P. Xu, M.-X. Wang, Z.-L. Liu, J.-F. Ge, X. Yang, C. Liu, Z. A. Xu, D. Guan, C. L. Gao, D. Qian, Y. Liu, Q.-H. Wang, F.-C. Zhang, Q.-K. Xue, and J.-F. Jia, Phys. Rev. Lett. **114**, 017001 (2015).

[9] S. Nadj-Perge, I. K. Drozdov, J. Li, H. Chen, S. Jeon, J. Seo, A. H. MacDonald, B. A. Bernevig, and A. Yazdani, Science **346**, 602 (2014).

[10] L. A. Wray, S.-Y. Xu, Y. Xia, Y. S. Hor, D. Qian, A. V. Fedorov, H. Lin, A. Bansil, R. J. Cava, and M. Z. Hasan, Nat. Phys. **6**, 855 (2010).

[11] Z. Liu, X. Yao, J. Shao, M. Zuo, L. Pi, S. Tan, C. Zhang, and Y. Zhang, J. Am. Chem. Soc. **137**, 10512 (2015).

[12] T. Asaba, B. J. Lawson, C. Tinsman, L. Chen, P. Corbae, G. Li, Y. Qiu, Y. S. Hor, L. Fu, and L. Li, Phys. Rev. X **7**, 011009 (2017).

[13] S. Sasaki, Z. Ren, A. A. Taskin, K. Segawa, L. Fu, and Y. Ando, Phys. Rev. Lett. **109**, 217004 (2012).

[14] M. Sakano, K. Okawa, M. Kanou, H. Sanjo, T. Okuda, T. Sasagawa, and K. Ishizaka, Nat. Commun. **6**, 8595 (2015).

[15] H.-J. Noh, J. Jeong, E.-J. Cho, K. Kim, B. I. Min, and B.-G. Park, Phys. Rev. Lett. **119**, 016401 (2017).

[16] M. N. Ali, Q. D. Gibson, T. Klimczuk, and R. J. Cava, Phys. Rev. B **89**, 020505 (2014).

[17] G. Bian, T.-R. Chang, R. Sankar, S.-Y. Xu, H. Zheng, T. Neupert, C.-K. Chiu, S.-M. Huang, G. Chang, I. Belopolski, D. S. Sanchez, M. Neupane, N. Alidoust, C. Liu, B. Wang, C.-C. Lee, H.-T. Jeng, C.-Z. Zhang, Z. Yuan, S. Jia, A. Bansil, F. Chou, H. Lin, and M. Z. Hasan, Nat. Commun. **7**, 10556 (2016).

[18] Z.-J. Wang, P. Zhang, G. Xu, L. K. Zeng, H. Miao, X.-Y. Xu, T. Qian, H.-M. Weng, P. Richard, A. V. Fedorov, H. Ding, X. Dai, and Z. Fang, Phys. Rev. B **92**, 115119 (2015).

[19] G. Xu, B. Lian, P.-Z. Tang, X.-L. Qi, and S.-C. Zhang, Phys. Rev. Lett. **117**, 047001 (2016).

[20] P. Zhang, K. Yaji, T. Hashimoto, Y. Ota, T. Kondo, K. Okazaki, Z. Wang, J. Wen, G. D. Gu, H. Ding, and S. Shin, Science **360**, 182 (2018).

[21] D.-F. Wang, L.-Y. Kong, P. Fan, H. Chen, S.-Y. Zhu, W.-Y. Liu, L. Cao, Y.-J. Sun, S.-X. Du, J. Schneeloch, R.-D. Zhong, G.-D. Gu, L. Fu, H. Ding, and H.-J. Gao, Science **362**, 333 (2018).

[22] M. Kim, C.-Z. Wang, and K.-M. Ho, arXiv:1807.03405.

[23] P. Hohenberg and W. Kohn, Phys. Rev. **136**, B864 (1964).

[24] W. Kohn and L. J. Sham, Phys. Rev. **140**, A1133 (1965).

[25] S. Baroni, S. de Gironcoli, A. Dal Corso, and P. Giannozzi, Rev. Mod. Phys. **73**, 515 (2001).

[26] P. Giannozzi *et al.*, J. Phys.: Condens. Matter **21**, 395502 (2009).

[27] N. Troullier and J. L. Martins, Phys. Rev. B **43**, 1993 (1991).

[28] J. P. Perdew, K. Burke, and M. Ernzerhof, Phys. Rev. Lett. **77**, 3865 (1996).

[29] S. Grimme, J. Comput. Chem. **27**, 1787 (2006).

[30] V. Barone, M. Casarin, Da. Forrer, M. Pavone, M. Sambi, and A. Vittadini, J. Comput. Chem. **30**, 934 (2009).

[31] Q. Wu, S. Zhang, H.-F. Song, M. Troyer, and A. A. Soluyanov, Comput. Phys. Commun. **224**, 405 (2018).

[32] J. Noffsinger, F. Giustino, B. D. Malone, C.-H. Park, S. G. Louie, and M. L. Cohen, Comput. Phys. Commun. **181**, 2140 (2010).

[33] A. A. Mostofi, J. R. Yates, G. Pizzi, Y.-S. Lee, I. Souza, D. Vanderbilt, and N. Marzari, Comput. Phys. Commun. **185**, 2309 (2014).

[34] G. M. Eliashberg, Zh. Eksp. Teor. Fiz. **38**, 966 (1960) [Sov. Phys. JETP **11**, 696 (1960)].

[35] P. B. Allen, Phys. Rev. B **6**, 2577 (1972).

[36] P. B. Allen and R. C. Dynes, Phys. Rev. B **12**, 905 (1975).

[37] C. F. Richardson and N. W. Ashcroft, Phys. Rev. Lett. **78**, 118 (1997).

[38] K.-H. Lee, K. J. Chang, and M. L. Cohen, Phys. Rev. B **52**, 1425 (1995).

[39] M. F. Gendron and R. E. Jones, J. Phys. Chem. Solids **23**, 405 (1962).

[40] A. Dal Corso, J. Phys.: Condens. Matter **20**, 445202 (2008).

[41] L. Fu and C. L. Kane, Phys. Rev. B **76**, 045302 (2007).

[42] A. D. Becke and E. R. Johnson, J. Chem. Phys. **124**, 221101 (2006).

[43] F. Tran and P. Blaha, Phys. Rev. Lett. **102**, 226401 (2009).

[44] J.-W. Sun, A. Ruzsinszky, and J. P. Perdew, Phys. Rev. Lett. **115**, 036402 (2015).

[45] J.-W. Sun, R. C. Remsing, Y.-B. Zhang, Z.-R. Sun, A. Ruzsinszky, H.-W. Peng, Z.-H. Yang, A. Paul, U. Waghmare, X.-F. Wu, M. L. Klein, and J. P. Perdew, Nat. Chem. **8**, 831 (2016).

[46] Y. S. Hor, A. J. Williams, J. G. Checkelsky, P. Roushan, J. Seo, Q. Xu, H. W. Zandbergen, A. Yazdani, N. P. Ong, and R. J. Cava, Phys. Rev. Lett. **104**, 057001 (2010).

[47] M. Novak, S. Sasaki, M. Kriener, K. Segawa, and Y. Ando, Phys. Rev. B **88**, 140502(R) (2013).

[48] R. D. Zhong, J. A. Schneeloch, X. Y. Shi, Z. J. Xu, C. Zhang, J. M. Tranquada, Q. Li, and G. D. Gu, Phys. Rev. B **88**, 020505(R) (2013).